Supplementary Information (SI) for Nanoscale.
This journal is © The Royal Society of Chemistry 2026

Enhancing Crystallization and Mechanical Properties of PET Polyester Using Functionalized Carbon Nanotubes

Pengwei Zhang[a], Yao Wang[a,] **, Miaorong Zhang[a], Linjun Huang[a], Kang Li[a], Feng Li[a], Wei Wang[a], Jianguo Tang[a,] *

[a] Institute of Hybrid Materials, National Center of International Research for Hybrid Materials Technology, National Base of International Science & Technology Cooperation, College of Materials Science and Engineering, Qingdao University, Qingdao 266071, P. R. China

* Corresponding author.

** Corresponding author.

E-mail addresses: tang@qdu.edu.cn (J. Tang), wangyaoqdu@126.com (Y. Wang).

Fig S1. TGA of CNTs，CNTs-OH and CNTs-APTES.

Fig S2. DSC cooling (a) and heating curves (b) of different concentrations of CNTs-APTES/PET；(c)The relative crystallinity X_t vs. crystallization time t-t_0 of different concentrations of CNTs-APTES/PET and the logarithm Avrami diagram ln[-$\ln^{1-Xt}$] vs. lnt of different concentrations of CNTs-APTES/PET.

Fig S3. The Shape of PET hybrid materials.

Fig S4. Data graph of elongation at break of CNTs-OH/PET and CNTs-APTES/PET.

Fig S5. Data graph of tensile sternghth of CNTs-OH/PET and CNTs-APTES/PET.

Fig S6. Data graph of modulus of CNTs-OH/PET and CNTs-APTES/PET.

Fig S7. Polarized optical microscopy images of the isothermal crystallization process of different PET-based composites at various temperatures.

Fig S8. Comparison of polarized optical microscopy images of the four PET-based composites after complete crystallization at 180° C.

Fig S9. Rheological behavior of the four PET-based composites at different temperatures: (a – c) Shear stress as a function of shear rate; (d) Shear stress vs. shear rate curves for CNTs-APTES/PET at various temperatures; (e – g) Viscosity as a function of shear rate; (h) Viscosity vs. shear rate curves for CNTs-APTES/PET at various temperatures.

Table S1. I_D/I_G of the original CNTs, CNTs-OH and CNTs-APTES.

Table S2. The relative percentage of the carbon and assignation.

Table S3.Thermal properties and non-isothermal kinetic analysis for CNTs-

APTES/PET.

Table S4. A comparison between the results of this paper and the published results.

Table S5. Non-isothermal crystallization kinetic parameters of different composite materials.

Table S6. Non-Newtonian index n of the four PET-based composites at different temperatures.

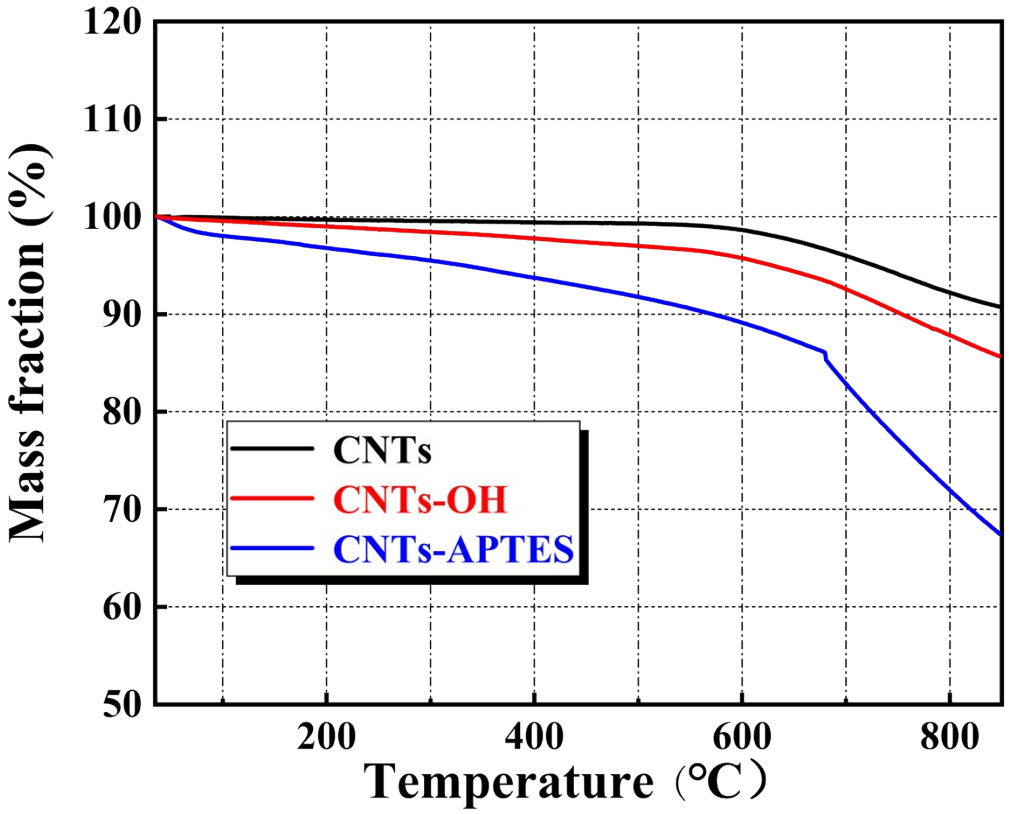

Fig S1. TGA of CNTs，CNTs-OH and CNTs-APTES.

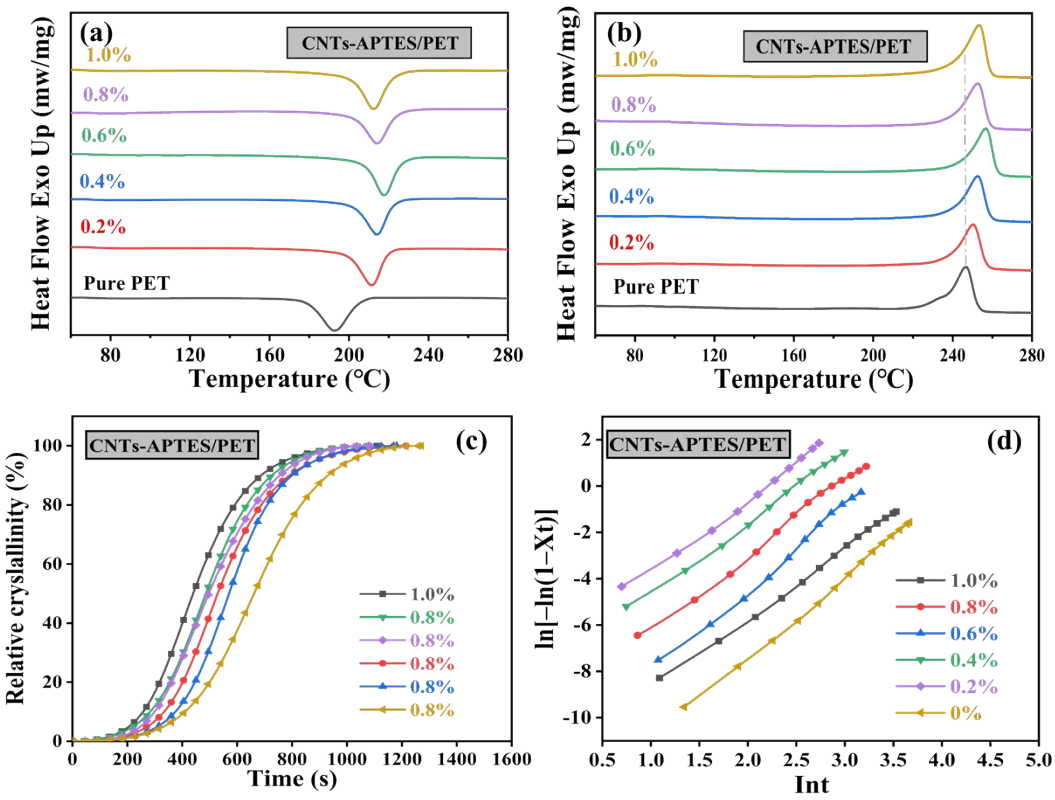

Fig S2. DSC cooling (a) and heating curves (b) of different concentrations of CNTs-APTES/PET; (c)The relative crystallinity X_t vs. crystallization time t-t_0 of different concentrations of CNTs-APTES/PET and the logarithm Avrami diagram ln[-$\ln^{1-Xt}$] vs. lnt of different concentrations of CNTs-APTES/PET.

Table S1.

I_D/I_G of the original CNTs, CNTs-OH and CNTs-APTES.

Sample	I_D/I_G
CNTs	0.70
CNTs-OH	1.11
CNTs-APTES	1.56

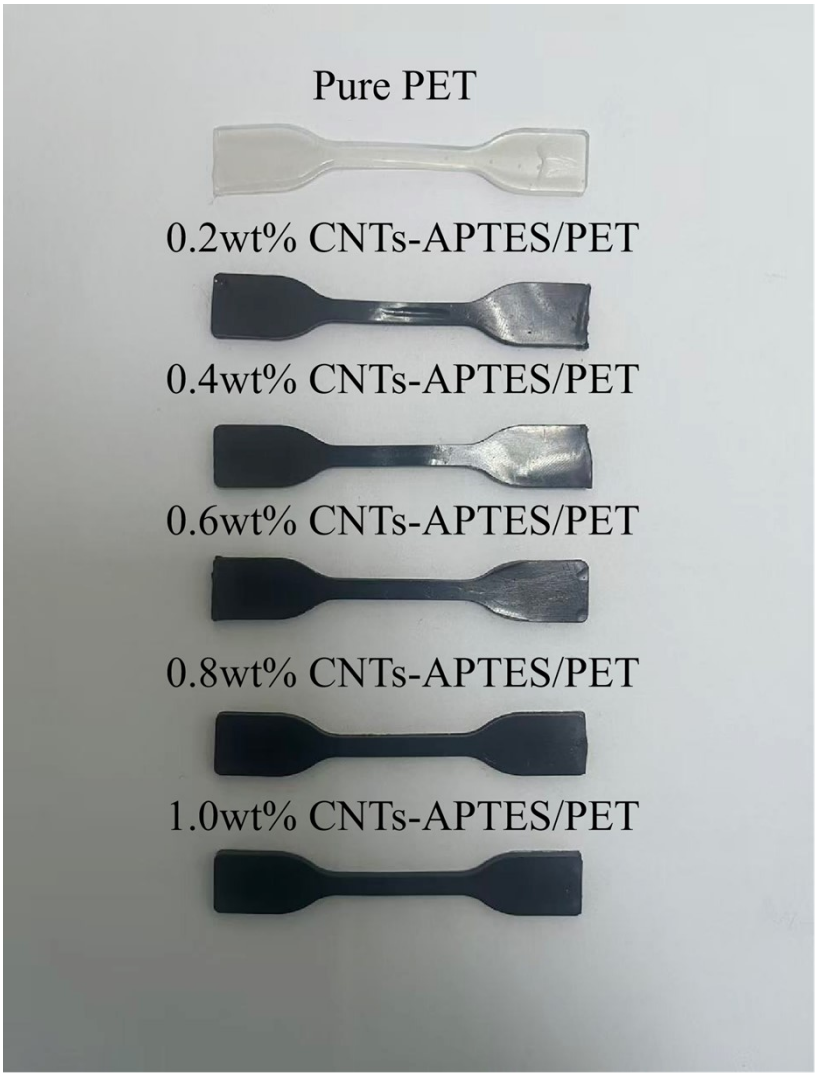

Fig S3. The Shape of PET hybrid materials.

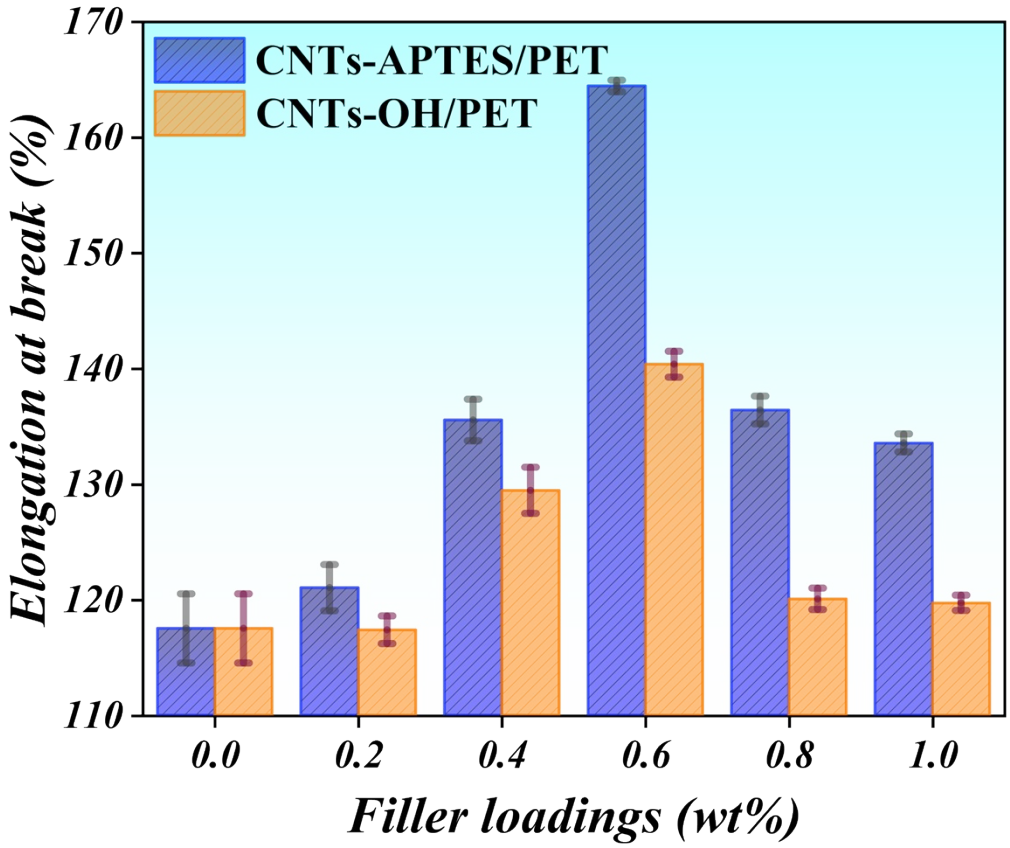

Fig S4. Data graph of elongation at break of CNTs-OH/PET and CNTs-APTES/PET.

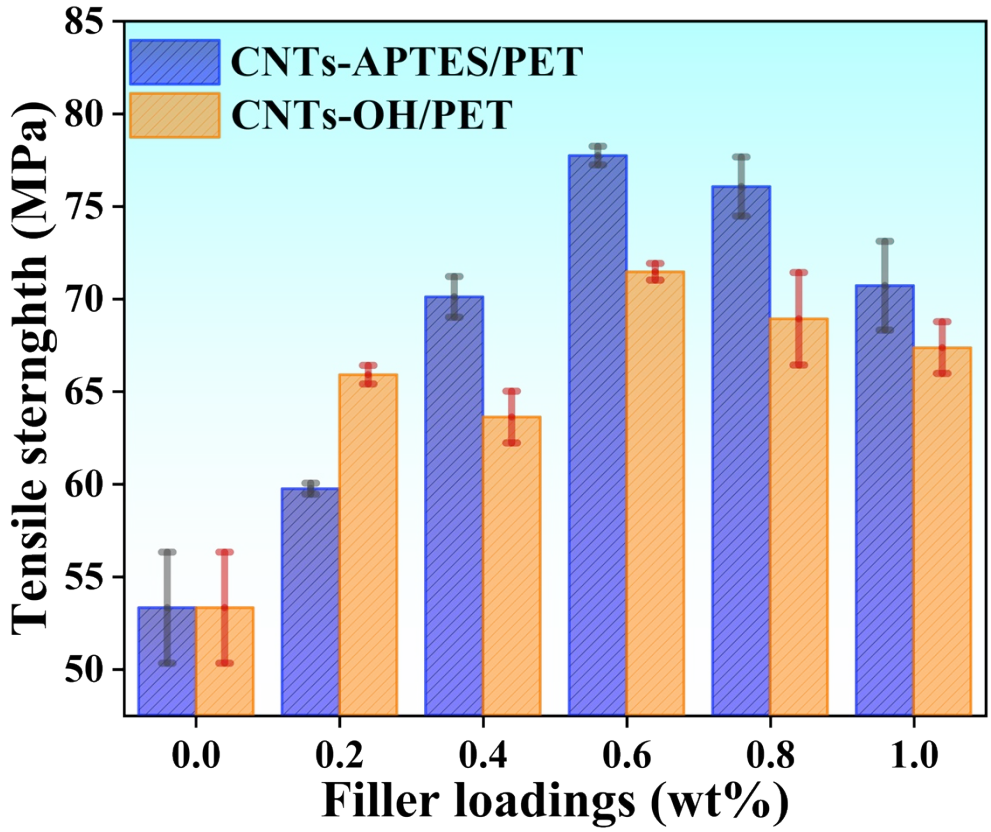

Fig S5. Data graph of tensile sternghth of CNTs-OH/PET and CNTs-APTES/PET.

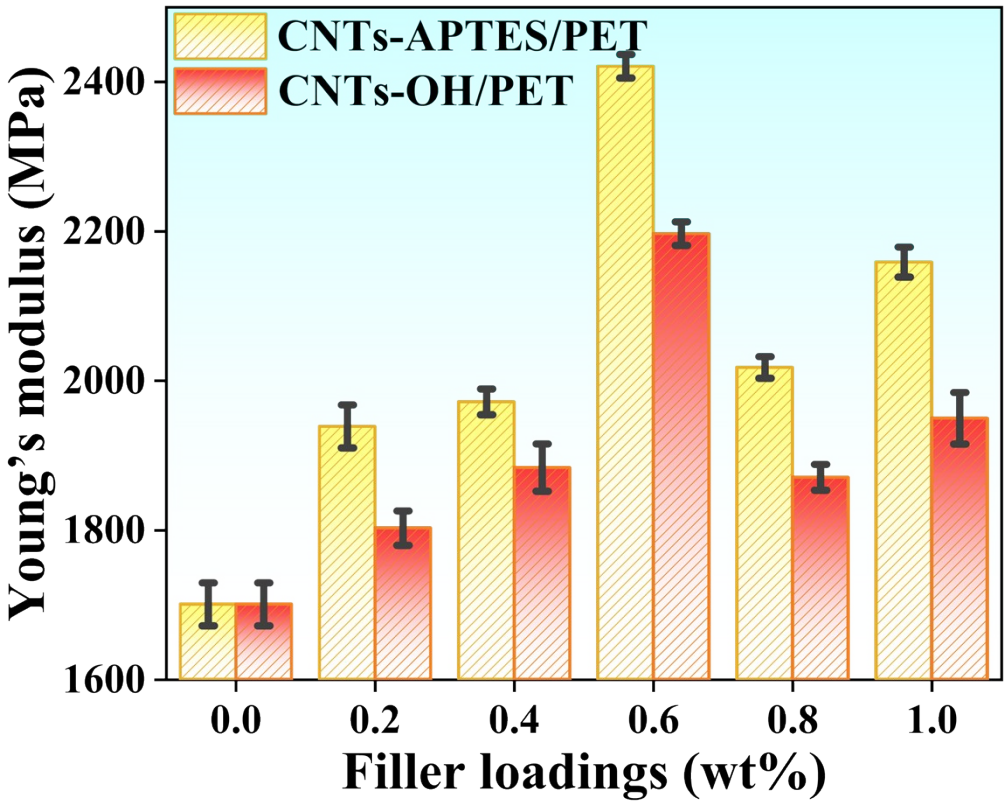

Fig S6. Data graph of modulus of CNTs-OH/PET and CNTs-APTES/PET.

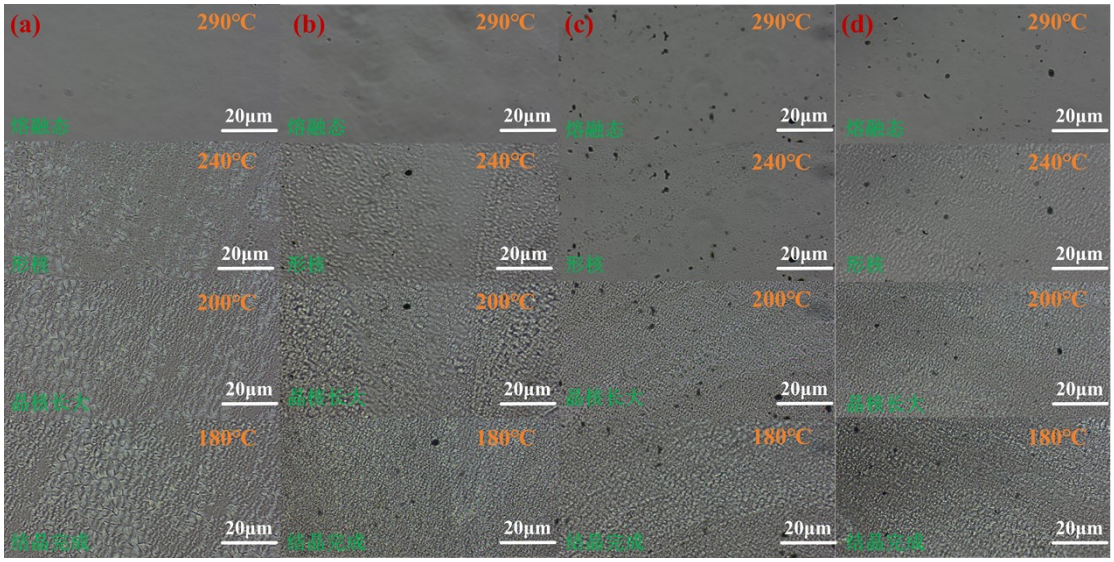

Fig S7. Polarized optical microscopy images of the isothermal crystallization process of different PET-based composites at various temperatures.

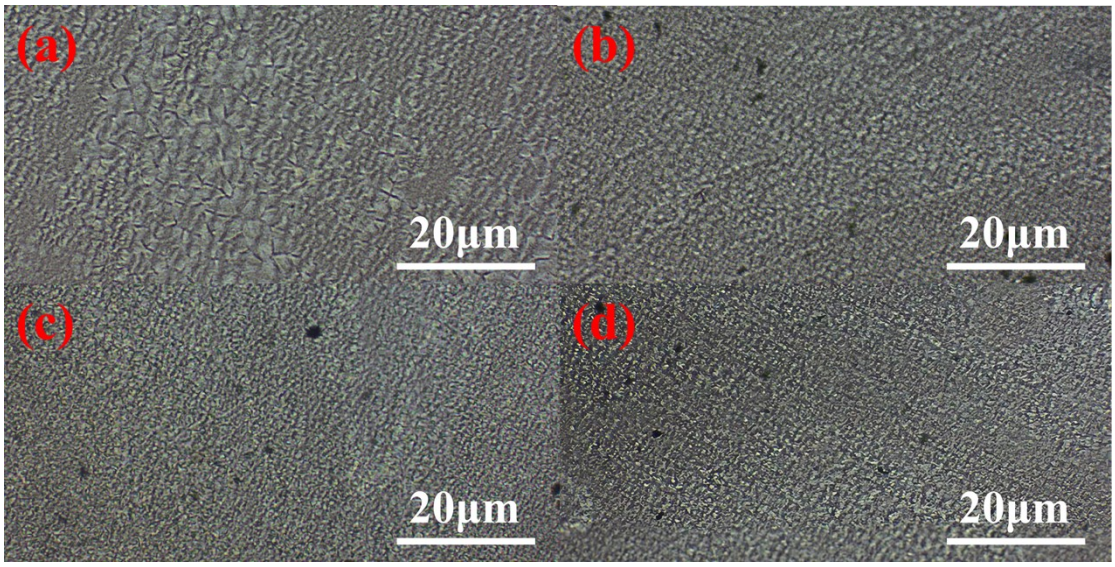

Fig S8. Comparison of polarized optical microscopy images of the four PET-based composites after complete crystallization at 180°C.

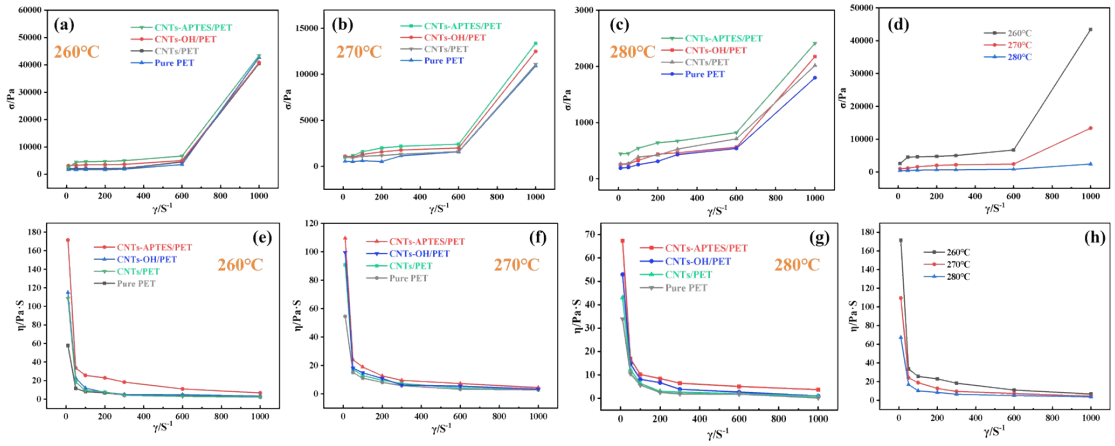

Fig S9. Rheological behavior of the four PET-based composites at different temperatures: (a–c) Shear stress as a function of shear rate; (d) Shear stress vs. shear rate curves for CNTs-APTES/PET at various temperatures; (e–g) Viscosity as a function of shear rate; (h) Viscosity vs. shear rate curves for CNTs-APTES/PET at various temperatures.

Table S2.

Characteristics of pristine CNTs, CNTs-OH and CNTs-APTES by XRD

Sample	CNTs	CNTs-OH	CNTs-APTES
peak location (2θ/°)	25.8	25.9	25.7
half-peak width (θ/°)	4.13	6.82	7.21

Table S3.

Thermal properties and non-isothermal kinetic analysis for CNTs-APTES/PET

Content(%)	T_c(℃)	T_m(℃)	T_g(℃)	ΔH_m(J/g)	ΔH_c(J/g)	X_t(%)	T(s)	n	K_c
Pure PET	192.9	246.4	71.5	28.04	26.82	20.0	665	3.09	0.40
0.2%CNTs-APTES/PET	211.4	250.1	73.9	43.06	34.77	30.8	568	3.03	0.52
0.4%CNTs-APTES/PET	214.1	252.6	78.0	42.36	39.12	30.2	502	2.97	0.54
0.6%CNTs-APTES/PET	218.4	257.1	81.7	50.59	46.36	36.1	407	2.73	0.58
0.8%CNTs-APTES/PET	214.3	252.5	77.4	43.13	39.72	30.8	495	2.91	0.55
1.0%CNTs-APTES/PET	212.2	253.2	75.2	40.28	35.96	28.8	520	3.01	0.51

0.6%CNTs/PET	210.2	250.4	79.2	44.61	40.36	31.9	535	2.87	0.52
0.6%CNTs-OH/PET	215.3	253.9	80.8	46.88	43.69	33.5	458	2.81	0.56

Table S4.

Non-Newtonian index n of the four PET-based composites at different temperatures.

sample.	**Temperature**		
	260℃	**270℃**	**280℃**
Pure PET	0.80	0.84	0.88
CNTs/PET	0.70	0.74	0.78
CNTs-OH/PET	0.62	0.66	0.70
CNTs-APTES/PET	0.50	0.55	0.60

Table S4.

A comparison between the results of this paper and the published results.

Performance Index	**Traditional Concentrated Acid Oxidation Method**	**This paper**	**Enhancement**

CNTs functionalization time	48 h + 24 h = 72 h	8 h + 12 h = 20 h	≈ 72.2% (original "90%" was a misstatement; revised to "reduced by ~72%" to align with actual data)
sp^2 carbon skeleton loss	>40% [21]	25.6% (XPS data in Section 3.2)	Loss reduced by 36%
PET tensile strength increase	~25% [34]	48.3%	Enhancement improved by 93%

Table S5.

Non-isothermal crystallization kinetic parameters of different composite materials

sample.	**Avrami exponent(n)**	**Crystallization rate constant Kt (min^{-1}).**	**Half-crystallization time $t_{1/2}$ (min).**
Pure PET	2.2±0.1	0.0023±0.0002	8.6±0.3
CNTs/PET	2.4±0.1	0.0035±0.0003	6.2±0.2
CNTs-OH/PET	2.6±0.1	0.0051±0.0003	5.3±0.2
CNTs-APTES/PET	2.9±0.1	0.0087±0.0003	5.2±0.1